On vortex rings around vortices: an optimal mechanism

ARNAUD ANTKOWIAK† AND PIERRE BRANCHER

Institut de Mécanique des Fluides de Toulouse (IMFT), 2, Allée du Professeur
Camille Soula, 31 400 Toulouse, France

Stable columnar vortices subject to hydrodynamic noise (e.g. turbulence) present recurrent behaviours, such as the systematic development of vortex rings at the periphery of the vortex core. This phenomenon lacks a comprehensive explanation, partly because it is not associated with an instability *stricto sensu*. The aim of the present paper is to identify the physical mechanism triggering this intrinsic feature of vortices using an optimal perturbation analysis as a tool of investigation. We find that the generation of vortex rings is linked to the intense and rapid amplification of specific disturbances in the form of azimuthal velocity streaks that eventually evolve into azimuthal vorticity rolls generated by the rotational part of the local Coriolis force. This evolution thus appears to follow a scenario opposite to the classical lift-up view, where rolls give rise to streaks.

1. Introduction

Vortices are ubiquitous in fluid flows, appearing in the tiniest scales of turbulence as well as in the largest geophysical ones. They have been the focus of considerable research effort over the past few decades. Partly motivated by industrial concerns related to the potential hazard of wing-tip vortices to following planes (e.g. see Stafford 2006), most of these studies aimed to depict the modal instabilities developing in vortices. As a result, several stability criteria have been elaborated in order to identify the candidates for an instability of centrifugal, inflectional (Gallaire & Chomaz 2003) or elliptic nature (Kerswell 2002). But some generic behaviours systematically exhibited by vortices still lack a convincing description. One can cite vortex bursting, a localized 'turbulent burst' affecting the vortex core while possibly travelling (Spalart 1998; Moet *et al.* 2005), vortex meandering, an erratic displacement of the vortex core occurring at large wavelengths (Devenport *et al.* 1996; Jacquin *et al.* 2005), or the systematic development of vortex rings at the periphery of vortices in both numerical simulations (Melander & Hussain 1993) and experiments (Beninati & Marshall 2005, and the references therein).

Similarly, in the context of plane shear flows, a phenomenon exhibited as a typical response of the flow in the presence of noise has long failed to be described with standard modal analyses. More specifically the emergence of elongated longitudinal velocity structures, or streaks, in response to an external forcing, is an intrinsic feature of shear flows. Furthermore, these streaks appear to play a key role in the transition process (Schmid & Henningson 2001). While standard analyses have failed in depicting

---

† Present address: IRPHÉ (Institut de Recherche sur les Phénomènes Hors Équilibre), Technopôle de Château-Gombert, 49, rue Joliot Curie, BP 146, 13 384 Marseille Cedex 13, France.

the mechanism of emergence of these recurrent patterns, alternative ideas, coined 'non-modal' in contrast to classical analyses, have reconsidered the concept of stability. Basically, by allowing disturbances to continuously deform while growing, these approaches have succeeded in identifying 'optimal' initial conditions that maximize their energy growth at a given time. Interestingly, these optimal disturbances exploit energy amplification mechanisms that are filtered out with traditional approaches. In particular, one of these mechanisms, the so-called 'lift-up effect' (Landahl 1975) is classically invoked to explain the emergence of streaks. This effect appears when studying the dynamics of an optimal disturbance in the form of rolls (of crossflow velocity components) which transform into strong streaks (or streamwise velocity variations). As such amplification mechanisms exploit specific properties of shear flows, one may expect that other mechanisms arise in the context of vortices, and are responsible for non-modal behaviours. Such behaviours were reported in Smith & Montgomery (1995) and Nolan & Farrell (1999) for two-dimensional vortex flows. Recently, Antkowiak & Brancher (2004) carried out an optimal perturbation analysis to examine these phenomena in the three-dimensional case, and found an intense core contamination mechanism. Pradeep & Hussain (2006) pursued this analysis and found evidence of axisymmetric transient growth for a non-diffusive vortex. They interpreted this behaviour in terms of tilting and stretching of vorticity (Kawahara *et al.* 1997), in line with the classical view of the emergence of vortex rings by the wrapping up of external vorticity and the merger of the wrapped-up structures.

Our goal in this work is to revisit the understanding of vortex rings formation at the periphery of vortices, a phenomenon so frequent that some simulations have mimicked the influence of turbulence on a vortex column by adding such surrounding vortex rings (Marshall 1998). Using tools that have proven to be successful in another context, we identify a simple physical mechanism that optimally promotes the emergence of vortex rings. This mechanism is specific to rotating flows and appears to act in a fashion that is the reverse of the classical lift-up effect, so that streaks (here corresponding to azimuthal velocity variations) now generate rolls (here azimuthal vortex rings) as an outcome. We therefore suggest that vortex rings emerge around vortices just as streaks naturally appear in shear flows.

2. A disturbed vortex

The flow considered in this article is the classical Lamb–Oseen Gaussian vortex, spreading under the action of viscosity. Using the characteristic scales Ω_0, the initial angular velocity at the vortex centre, r_0, the initial dispersion radius of the vortex, and ν, the kinematic viscosity, we can express the vorticity $Z(r, t)$ and the angular velocity $\Omega(r, t)$ in the following non-dimensional form:

$$Z(r, t) = \frac{2}{1 + 4t/Re} \exp(-r^2/(1 + 4t/Re)), \quad \Omega(r, t) = \frac{1 - \exp(-r^2/(1 + 4t/Re))}{r^2}.$$

The Reynolds number defined with these characteristic scales,

$$Re = \frac{\Omega_0 r_0^2}{\nu} = \frac{\Gamma}{2\pi\nu}, \tag{2.1}$$

is the only control parameter of the flow. Here, Γ is the circulation of the vortex.

In order to identify the perturbation with the most growth, the evolution equations for an arbitrary disturbance have first to be derived (Fabre, Sipp & Jacquin 2006). In the classical cylindrical coordinates (r, θ, z), a general hydrodynamic disturbance is

described by its velocity field $\boldsymbol{u} = (u_r, u_\theta, u_z)$ and pressure p. Expressing u_z and then p as functions of u_r and u_θ, it is possible to write the whole initial value problem for this reduced set of variables:

$$\boldsymbol{F}(\boldsymbol{u}) = \boldsymbol{L}\frac{\partial \boldsymbol{u}}{\partial t} + \boldsymbol{C}\boldsymbol{u} - \frac{1}{Re}\boldsymbol{D}\boldsymbol{u} = 0 \tag{2.2}$$

Restricting the scope of this study to axisymmetric disturbances, and considering normal mode disturbances of the form $f(r, t)\mathrm{e}^{\mathrm{i}kz}$, the following expressions for operators $\boldsymbol{L}$, $\boldsymbol{C}$ and $\boldsymbol{D}$ hold:

$$\boldsymbol{L} = \begin{pmatrix} \delta_k & 0 \\ 0 & 1 \end{pmatrix}, \qquad \boldsymbol{C} = \begin{pmatrix} 0 & -2\Omega \\ Z & 0 \end{pmatrix}, \qquad \boldsymbol{D} = \begin{pmatrix} \Delta_k\delta_k & 0 \\ 0 & \Delta_k \end{pmatrix}, \tag{2.3}$$

where

$$\Delta_k = \frac{\partial^2}{\partial r^2} + \frac{1}{r}\frac{\partial}{\partial r} - \frac{1}{r^2} - k^2 \quad \text{and} \quad \delta_k = 1 - \frac{1}{k^2}\Delta_0. \tag{2.4}$$

For a given disturbance, classically we consider the kinetic energy contained in a cylinder of height one wavelength and of infinite radius. Normalized with the factor $k/4\pi^2$, it can be expressed as:

$$E(t) = \frac{1}{2}\int_0^\infty (\bar{u}_r u_r + \bar{u}_\theta u_\theta + \bar{u}_z u_z)r\,\mathrm{d}r = \frac{1}{4}(\boldsymbol{L}\boldsymbol{u}, \boldsymbol{u}) \tag{2.5}$$

where an overbar stands for complex conjugation, and where the scalar product $(\boldsymbol{a}, \boldsymbol{b})$ is defined as $\int_0^\infty \bar{\boldsymbol{a}}^T \boldsymbol{b}\ r\,\mathrm{d}r +$ c.c.

3. Some technical background

In the present work, the general framework for the optimal perturbation identification described in Corbett & Bottaro (2001) has been adopted. This optimal control-theory-based strategy presents the advantage of not requiring the steadiness of the flow. As this technique is now classical, only a brief outline will be presented in the following.

A classical variational formulation of the problem is employed to identify the initial condition inducing the most growth. To this end, it proves useful to introduce $\boldsymbol{u}_0$, the form of the perturbation at initial time of energy E_0, so that $\boldsymbol{u}$ and $\boldsymbol{u}_0$ are now related through the relation

$$\boldsymbol{H}(\boldsymbol{u}, \boldsymbol{u}_0) = \boldsymbol{u}(0) - \boldsymbol{u}_0 = 0. \tag{3.1}$$

The optimal perturbation is then the particular initial condition maximizing the energy growth

$$G(\tau) = \frac{E(\tau)}{E_0} \tag{3.2}$$

at a given time τ. Equivalently, the optimal perturbation is the particular $\boldsymbol{u}_0$ maximizing the functional

$$\mathscr{I}(\boldsymbol{u}_0, \boldsymbol{u}) = G(\tau), \tag{3.3}$$

subjected to the constraints $\boldsymbol{F}(\boldsymbol{u}) = 0$ and $\boldsymbol{H}(\boldsymbol{u}, \boldsymbol{u}_0) = 0$. The constrained optimization problem is circumvented by introducing the Lagrange functional

$$\mathscr{L}(\boldsymbol{u}, \boldsymbol{u}_0, \boldsymbol{a}, \boldsymbol{c}) = \mathscr{I}(\boldsymbol{u}, \boldsymbol{u}_0) - \langle \boldsymbol{F}(\boldsymbol{u}), \boldsymbol{a}\rangle - (\boldsymbol{H}(\boldsymbol{u}, \boldsymbol{u}_0), \boldsymbol{c}), \tag{3.4}$$

already including the constraints by means of appropriate Lagrange multipliers. Here the scalar product $\langle \boldsymbol{a}, \boldsymbol{b}\rangle$ is defined as $\int_0^\tau \int_0^\infty \bar{\boldsymbol{a}}^T \boldsymbol{b}\ r\,\mathrm{d}r\,\mathrm{d}t +$ c.c.

At a stationary point, the directional derivatives of $\mathscr{L}$ vanish. More specifically, the cancellation of these derivatives with respect to a and c allows the constraints (2.2) and (3.1) to be recovered, as expected. The condition for the gradient with respect to u to vanish implies that a satisfies the following adjoint equation:

$$F^+(a) = -L\frac{\partial a}{\partial t} + C^+a - \frac{1}{Re}Da = 0, \qquad (3.5)$$

revealing this Lagrange muliplier as an adjoint variable. Here operator C^+ is expressed as

$$C^+ = \begin{pmatrix} 0 & Z \\ -2\Omega & 0 \end{pmatrix}. \qquad (3.6)$$

Cancelling the u derivative of $\mathscr{L}$ provides transfer relations between the adjoint and direct spaces. Finally, the gradient of the functional with respect to the control can be written

$$\nabla_{u_0}\mathscr{I} = -2\frac{E(\tau)}{E_0^2}u_0 + a(0). \qquad (3.7)$$

For a given u_0, $a(0)$, computed at the expense of successive integrations of the direct and adjoint equations, allows the functional gradient to be determined. Different strategies can then be elaborated to improve the control, for example the elementary fixed step gradient procedure used in this study.

The preceding approach is designed to identify the initial condition maximizing energy growth at a fixed time τ. A second step may consist in looking for the optimal time τ_{opt}, the result of an optimization with respect to time. The corresponding initial condition is then called a global optimal perturbation, or, in short, the optimal perturbation. In some cases, it will be of interest to find the optimal perturbation corresponding to fixed time $\tau < \tau_{\mathrm{opt}}$. In that case, the corresponding optimal perturbation will be termed a short-term optimal (Corbett & Bottaro 2001).

In the numerical treatment of the problem, the spatial derivatives are approximated with a Chebyshev pseudospectral method (e.g. Fornberg 1995), where the Gauss–Lobatto grid is algebraically mapped onto the semi-infinite physical space. The parity of the functions is taken into account in the expression of the derivatives (Kerswell & Davey 1996). All calculations are carried out using MATLAB and the DMSuite package developed by Weideman & Reddy (2000).

4. Axisymmetric amplification

4.1. *Quantitative overview*

Figure 1 reports the maximal growths achieved with axisymmetric disturbances. It can already be seen that considerable energy amplification (of order of 10^4) is obtained, though asymptotic exponential decay is predicted with modal analysis. The plot also reveals that large amplification occurs especially at large axial wavelengths. In this limit, the amplification is accompanied by a tendency for the optimal time τ_{opt} to diverge.

4.2. *A note on the $k \to 0$ limit*

The behaviour of energy growth near the bidimensional limit $k = 0$ deserves comment. It is useful to stress again that unlike classical linear stability analyses, the present study does not require 'freezing' the diffusion of the base flow. With viscous diffusion taken into account, the present results are therefore valid whatever the time scale of amplification (which can be of order of a thousand periods of rotation of the vortex
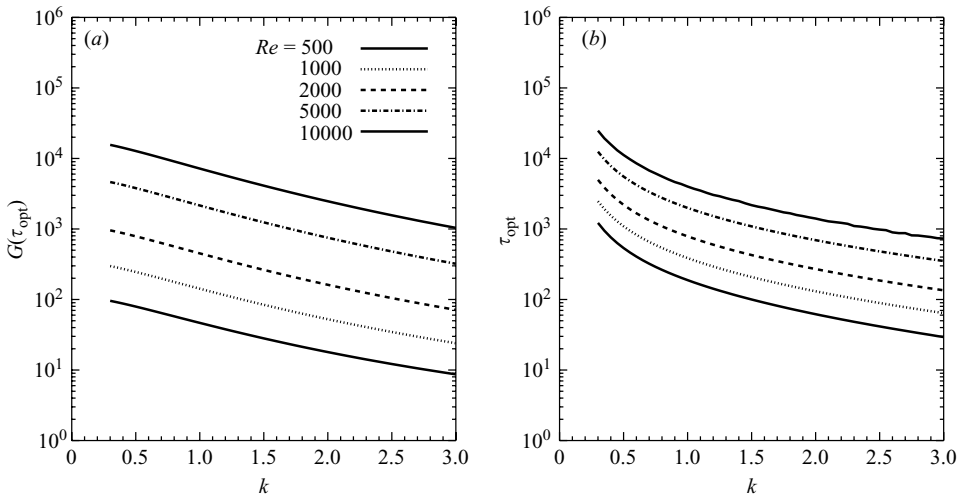
FIGURE 1. (*a*) Maximal amplification reached with axisymmetric optimal perturbations, as a function of the axial wavenumber k. (*b*) Corresponding optimal time.
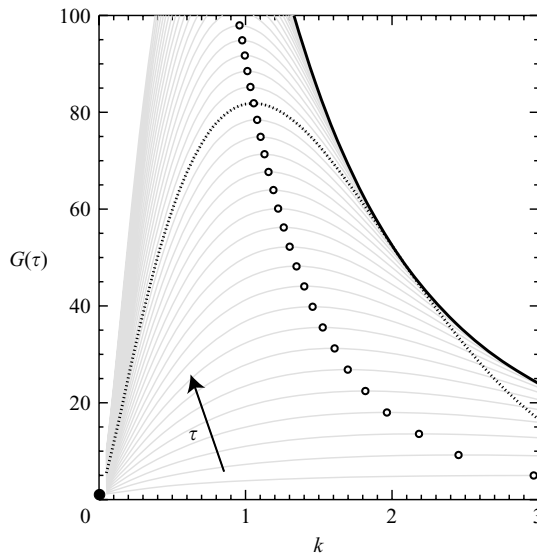

FIGURE 2. $Re = 1000$. Amplification curves associated with the short-term optimals for optimization times $\tau = 1, 2 \ldots 40$ rotation periods of the vortex. The computations have been carried out as long as $\tau < \tau_{opt}$, except for $\tau = 20$ where the whole curve is represented for all k (dotted curve). The optimal wavenumber k_{max} is shown on each curve with an open circle, and the filled circle shows the theoretical limit $G(k=0) = 1$.

core in the present case). Another comment associated with these results is the fact that no amplification can occur in the exact two-dimensional limit. Basically this limit corresponds to a slight modification of the base vorticity profile, and is therefore subjected to the same diffusion mechanism and time scale as the base flow. The mathematical counterpart of this statement is the self-adjointness of the governing operator in this limit, or, alternatively, the cancellation of the production term in the energy equation due to the vanishing of radial velocity (Smith & Montgomery 1995; Pradeep & Hussain 2006). $G(k=0, t=0) = 1$ therefore constitutes an upper bound

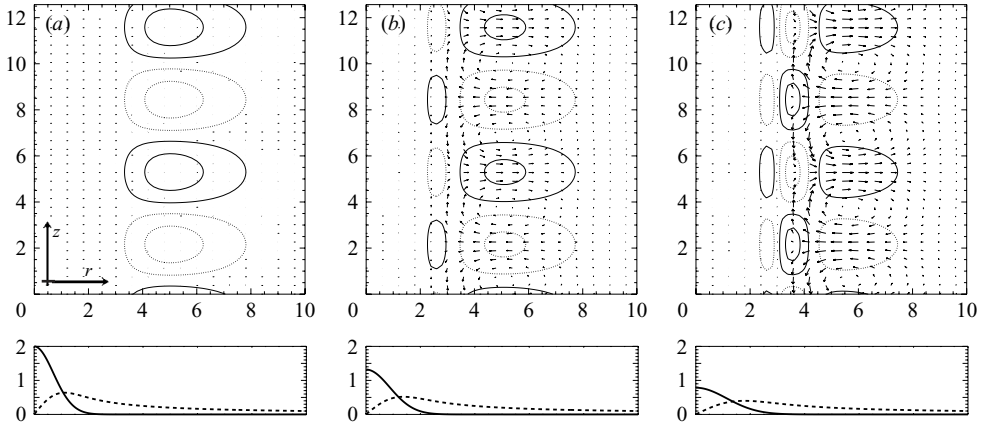FIGURE 3. $k = 1$, $Re = 1000$. Evolution of a typical optimal disturbance. (*a*) $t = 0$, (*b*) $t = \tau_{opt}/3$ and (*c*) $t = \tau_{opt}$. The contours represent the azimuthal velocity u_θ level (solid: positive, dotted: negative). The velocity field represents the velocity components u_r and u_z of the perturbation. The diffusive base flow is plotted underneath (solid: vorticity, dotted: azimuthal velocity).

for the energy growth $G(k = 0, t)$. But this behaviour is associated with a singular limit, as shown in figure 2, which plots the amplification curves obtained with initial conditions maximizing their energy at a fixed time $\tau < \tau_{opt}$, or 'short-term optimals' as coined by Corbett & Bottaro (2001). It appears clearly that there is selection of a particular wavenumber k_{max} corresponding to the largest energy growth at a given time depending on the time of optimization τ. As τ is progressively increased, a drift of this maximum wavenumber to larger wavelengths is observed. But in the same time, the energy growth in the bidimensional limit is still less than 1. Thus, the amplification curve becomes increasingly steep near $k = 0$, allowing large energy excursion for large-wavelength structures† while preserving the 'no growth' condition in the two-dimensional case.

4.3. *Structure of the optimal perturbation*

Figure 3 shows the typical evolution of an optimal initial condition. The perturbation is initially composed of a stack of azimuthal velocity streaks located outside the vortex core, in the quasi-potential zone. Interestingly, this distribution of azimuthal velocity streaks is exponentially localized, and therefore does not change the overall circulation budget. As time evolves, the structure of the optimal perturbation evolves in turn (recall that this perturbation is not of modal type) and vortex rings (azimuthal vorticity tori) of alternate signs form and become increasingly stronger. In the evolution depicted figure 3, the intensification of the vortex rolls is at the expense of the initial velocity streaks, which slowly diffuse. By the end of the sequence, the vortex rings contain almost all the energy.

It might be interesting to compare this evolution to the lift-up effect in plane shear flows that transforms initially weak streamwise rolls into powerful streamwise streaks. Conversely, the present optimal initial condition consists of a set of azimuthal (streamwise) velocity streaks that evolves into a stack of strong vortex rings (streamwise rolls). For convenience, we will therefore denote this counterintuitive

---

† An analogous behaviour in diffusing plane shear flow has been reported in Luchini (1996).

evolution the 'anti-lift-up' scenario. The associated physical mechanism is investigated in the following and explained in terms of ingredients specific to swirling flows.

5. The physical mechanism

Two views will be successively adopted in the following. First, based on momentum conservation equations, the interplay between velocity streaks and vortex rings will be made explicit, as well as its time dependence. Secondly, a physical picture of the emergence of vortex rings will be proposed based on angular momentum conservation. Both complementary views will allow further insight into this simple but non-trivial phenomenon.

Localized outside the vortex core, the optimal initial condition evolves in a region that can reasonably be considered as potential. Without base vorticity, the azimuthal velocity perturbation obeys a pure diffusion equation:

$$\frac{\partial u_\theta}{\partial t} = \frac{1}{Re} \Delta u_\theta. \tag{5.1}$$

Similarly, taking the azimuthal projection of the Helmholtz equation for vorticity, we are left with the following evolution equation for the vortex rings:

$$\frac{\partial \omega_\theta}{\partial t} = 2\Omega(r, t) \frac{\partial u_\theta}{\partial z} + \frac{1}{Re} \Delta \omega_\theta. \tag{5.2}$$

Whereas the streaks evolve free of any hydrodynamic feedback, the vortex rings are completely driven by the streaks. From equation (5.2), which could alternatively be interpreted in terms of standard tilting and stretching arguments (Pradeep & Hussain 2006), it can be seen that the vortex rings development follows a linear time dependence in the inviscid limit (except in the bidimensional limit where the expected decay is obvious from (5.1) and (5.2)). Again, this algebraic time dependence, although simple, is completely filtered out with standard modal arguments (Ellingsen & Palm 1975).

A further insight into the amplification mechanism may now be given, taking an alternative view based on angular momentum conservation arguments. The Lamb–Oseen vortex corresponds to an equilibrium where the centrifugal force acting on fluid particles is balanced by the pressure gradient. Introduction of a perturbation disturbs this equilibrium. More precisely, a fluid particle subjected to an azimuthal velocity disturbance u_θ will drift radially under the action of the local Coriolis force $\boldsymbol{F}_{\mathrm{coriolis}} = 2\Omega(r, t)u_\theta \boldsymbol{e}_r$. Indeed, following Batchelor (1967, § 3.2) it can be easily shown that in a frame corotating with the fluid located at r, we have

$$\frac{\partial u_r}{\partial t} = -\frac{\partial p}{\partial r} + 2\Omega(r, t)u_\theta + \frac{1}{Re}(\Delta \boldsymbol{u}) \cdot \boldsymbol{e}_r \tag{5.3}$$

where u_θ represents the same hydrodynamic disturbance as the one in the fixed frame due to axisymmetry, and the term $2\Omega(r, t)u_\theta$ explicitly originates from the Coriolis force. Thus, if located in a high-velocity streak the fluid particle will be expelled radially outwards, while it will be pushed to the centre-axis if the streak is a low-velocity region. Generalizing this reasoning for each fluid particle, it is possible to construct figure 4(*a*). This alternative view of the initial condition represents the local Coriolis force field acting in the fluid at initial time. Since an azimuthal velocity perturbation is purely diffusing in the potential region, it becomes possible to see the initial stack of streaks as an inhomogeneous distribution of local Coriolis body force, fixed in the bulk and slowly diffusing, with momentum diffusivity.
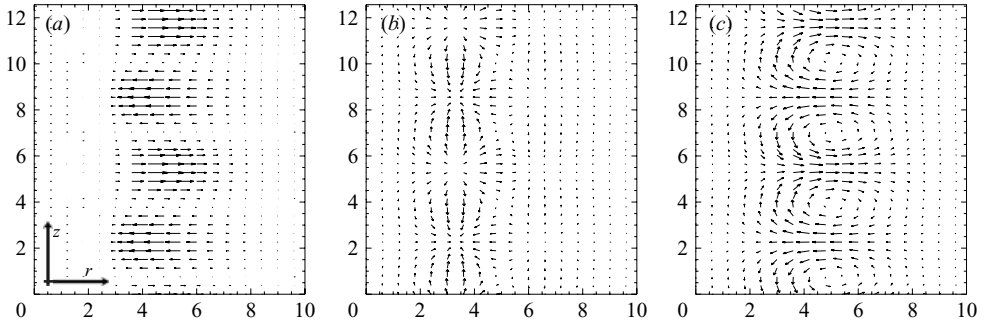
FIGURE 4. $k = 1$, $Re = 1000$. (a) 'Coriolisogram' of the optimal initial condition and its Helmholtz decomposition into (b) potential and (c) rotational parts.

But so far, the collective behaviour of the particles has been neglected, and the 'Coriolisogram' proposed only offers a partial view of the mechanism. Hydrodynamic interactions between particles can be investigated by taking the divergence of the governing equations. This results in the following Poisson equation for the pressure field p:

$$\Delta p = \frac{1}{r}\frac{\partial}{\partial r}(2r\Omega(r,t)u_\theta), \qquad (5.4)$$

which can be solved numerically, with an appropriate shooting method for example. The signification of equation (5.4) is made clearer if one recognizes the divergence of the Coriolis force on the right-hand side. It should now be evident that the pressure force $-\nabla p$ is the opposite of the Coriolis force's potential part. Physically, the equivalent body force field in figure 4(a) induces compression and dilation of fluid particles, which are not allowed in the incompressible evolution considered here. Pressure enforces incompressibility by cancelling the potential part of the Coriolis force (figure 4b). As a result, the effective force field acting on fluid particles is the rotational part of the Coriolis force (figure 4c), a result readily visible through the azimuthal vorticity evolution equation (5.2) where the first term of the right-hand side is $(\nabla \times \boldsymbol{F}_{\mathrm{coriolis}}) \cdot \boldsymbol{e}_\theta$. (Note that in the bidimensional limit, the rotational part of the Coriolis force vanishes.) *In summary, the evolution of the optimal perturbation and the underlying mechanism can be explained on the basis of simple physical arguments: the initial streaks of azimuthal velocity generate a distribution of Coriolis force whose rotational part is responsible for the production of azimuthal vorticity and the subsequent emergence of vortex rings.*

The physical understanding of the amplification mechanism allows insight into its scaling laws. According to equation (5.1), an azimuthal velocity streak of amplitude $O(\varepsilon)$ stays fixed in the fluid on a time scale $O(Re)$. Vortex rings are slaves of the streaks, as shown with equation (5.2), and encounter an amplification stage bringing them to an amplitude $O(\varepsilon Re)$. As for the lift-up effect, a Re^2 scaling for the energy is thus expected. Rescaling the optimal times of figure 1(b), it can be shown that the diffusive time scale is exactly verified. But so far, the scaling predicted for the energy growth appears to be an upper bound. The base vorticity, neglected in the present analysis, is responsible for the alteration of the scaling law (Antkowiak 2005; Pradeep & Hussain 2006). Indeed, the Re^2 scaling has been rigorously verified in an unpublished study conducted by the first author and Michel Rieutord in the case of vanishing epicyclic frequency (i.e. potential) Taylor–Couette flow.

6. Conclusions

A powerful mechanism of disturbance energy amplification has been found in vortices. Particular initial conditions that optimally exploit this effect have been exhibited, and their dynamics decrypted. Such optimal disturbances are typically composed of a stack of azimuthal velocity streaks at the initial time. As time evolves, this arrangement of streaks continuously deforms and transforms into a set of contrarotating vortex rings wrapped around the vortex core. The whole process is characterized by a strong amplification of disturbance kinetic energy, even at moderate Reynolds numbers. Moreover this amplification scales as Re^2 in the ideal limit of potential base flow, whereas the optimal time follows a diffusive Re time scale. These scalings, as well as the structures involved (longitudinal streaks and rolls), have properties analogous with the lift-up phenomenon occurring in plane shear flows. It must be stressed that these two phenomena act in a reverse fashion, and are based on totally different physical ingredients: whereas a shearwise disturbance (roll) exploits the ambient shear to induce large longitudinal deviations (streaks) in a vortical layer, an azimuthal velocity disturbance (streak) injected in a potential rotating flow exploits the ambient rotation and triggers the development of intense vortex rings (rolls) as a consequence of angular momentum conservation through the generation of a particular distribution of Coriolis force.

This mechanism is generic in two ways. On the one hand, it does not depend on the core vorticity profile, as it is active in the quasi-potential part of the flow. On the other hand, though shown with a particular perturbation profile here, it will be activated by any azimuthal velocity disturbance localized outside the vortex core. In particular, a continuous random forcing should exploit the underlying physical mechanism presented here. Eventually, the result of the optimal perturbation (sometimes termed a 'pseudomode') should emerge from the noise, as demonstrated in the case of plane shear flows (Farrell & Ioannou 1993). Obviously, this conjecture has to be confirmed with a proper stochastic forcing analysis, which is currently under way (some former RDT analyses conducted on vortices are already clues of such behaviours, see Miyazaki & Hunt 2000). If confirmed, this scenario would explain the propensity of vortices to develop characteristic vortex ring structures at their periphery when submerged in a disturbed environment such as a turbulent background.

Another result of the present study raises some questions about standard modal stability analyses of vortices. These assume on the one hand that transients have died away (asymptotic long time analysis), but require on the other hand the steadiness of the flow. This latter assumption implicitly restricts the validity in time of such analyses, the diffusive time scale $O(Re)$ being an upper bound. Conversely, the present work, considering the viscous spreading of the vortex, shows that transients may exist, if not arise, precisely on this diffusive time scale. Therefore these results suggest that care should be taken with predictions obtained with modal approaches, at least regarding the evolution of axisymmetric perturbations.

Finally, an interesting mechanism that is undetectable with standard approaches has been shown in vortices, using the optimal perturbation identification as a tool of investigation. This mechanism is specific to rotating flows and is not just a variant of well-known plane shear flows mechanisms. As illustrated here, the optimal perturbation analysis thus provides with a useful framework for revealing original physical mechanisms that exploit the intrinsic properties of the flow: shear or differential rotation, but also potentially stratification, surface tension, etc.

REFERENCES

ANTKOWIAK, A. 2005 Dynamique aux temps courts d'un tourbillon isolé. PhD thesis, Université Paul Sabatier, Toulouse, France.

ANTKOWIAK, A. & BRANCHER, P. 2004 Transient energy growth for the Lamb-Oseen vortex. *Phys. Fluids* **16** (1), L1–L4.

BATCHELOR, G. K. 1967 *An Introduction to Fluid Dynamics*. Cambridge University Press.

BENINATI, M. L. & MARSHALL, J. S. 2005 An experimental study of the effect of free-stream turbulence on an trailing vortex. *Exps. Fluids* **38**, 244–257.

CORBETT, P. & BOTTARO, A. 2001 Optimal linear growth in swept boundary layers. *J. Fluid Mech.* **435**, 1–23.

DEVENPORT, W. J., RIFE, M. C., LIAPIS, S. I. & FOLLIN, G. J. 1996 The structure and development of a wing-tip vortex. *J. Fluid Mech.* **312**, 67–106.

ELLINGSEN, T. & PALM, E. 1975 Stability of linear flow. *Phys. Fluids* **18** (4), 487–488.

FABRE, D., SIPP, D. & JACQUIN, L. 2006 The Kelvin waves of a Lamb-Oseen vortex. *J. Fluid Mech.* **551**, 235–274.

FARRELL, B. F. & IOANNOU, P. J. 1993 Stochastic forcing of the linearized Navier-Stokes equations. *Phys. Fluids* **5** (11), 2600–2609.

FORNBERG, B. 1995 *A Practical Guide to Pseudospectral Methods*. Cambridge University Press.

GALLAIRE, F. & CHOMAZ, J.-M. 2003 Three-dimensional instability of isolated vortices. *Phys. Fluids* **15** (8), 2113–2126.

JACQUIN, L., FABRE, D., SIPP, D. & COUSTOLS, E. 2005 Unsteadiness, instability and turbulence in trailing vortices. *C. R. Physique* **6**, 399–414.

KAWAHARA, G., KIDA, S., TANAKA, M. & YANASE, S. 1997 Wrap, tilt and stretch of vortex lines around a strong thin straight vortex tube in a simple shear flow. *J. Fluid Mech.* **353**, 115–162.

KERSWELL, R. R. 2002 Elliptical instability. *Annu. Rev. Fluid Mech.* **34**, 83–113.

KERSWELL, R. R. & DAVEY, A. 1996 On the linear instability of elliptic pipe flow. *J. Fluid Mech.* **316**, 307–324.

LANDAHL, M. T. 1975 Wave breakdown and turbulence. *SIAM J. Appl. Maths* **28** (4), 735–756.

LUCHINI, P. 1996 Reynolds-number-independent instability of the boundary layer over a flat surface. *J. Fluid Mech.* **327**, 101–115.

MARSHALL, J. S. 1998 A model of heavy particle dispersion by organized vortex structures wrapped around a columnar vortex core. *Phys. Fluids* **10** (12), 3236–3238.

MELANDER, M. V. & HUSSAIN, F. 1993 Coupling between a coherent structure and fine-scale turbulence. *Phys. Rev.* E **48** (4), 2669–2689.

MIYAZAKI, T. & HUNT, J. C. R. 2000 Linear and nonlinear interactions between a columnar vortex and external turbulence. *J. Fluid Mech.* **402**, 349–378.

MOET, H., LAPORTE, F., CHEVALIER, G. & POINSOT, T. 2005 Wave propagation in vortices and vortex bursting. *Phys. Fluids* **17**, 054109.

NOLAN, D. S. & FARRELL, B. F. 1999 Generalized stability analyses of asymmetric disturbances in one- and two-celled vortices maintained by radial inflow. *J. Atmos. Sci.* **56**, 1282–1307.

PRADEEP, D. S. & HUSSAIN, F. 2006 Transient growth of perturbations in a vortex column. *J. Fluid Mech.* **550**, 251–288.

SCHMID, P. J. & HENNINGSON, D. S. 2001 *Stability and Transition in Shear Flows*. Springer.

SMITH, G. B. & MONTGOMERY, M. T. 1995 Vortex axisymmetrization: Dependance on azimuthal wave-number or asymmetric radial structure changes. *Q. J. R. Meteorol. Soc.* **121**, 1615–1650.

SPALART, P. R. 1998 Airplane trailing vortices. *Annu. Rev. Fluid Mech.* **30**, 107–138.

STAFFORD, N. 2006 Turbulent times. *Nature* **443**, 385.

WEIDEMAN, J. A. C. & REDDY, S. C. 2000 A MATLAB differentiation matrix suite. *ACM Trans. Math. Soft.* **26** (4), 465–519.